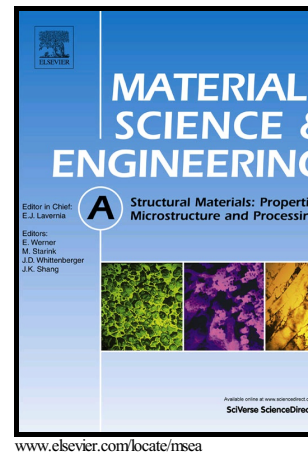# Author's Accepted Manuscript

FIB/FESEM experimental and analytical assessment of R-curve behavior of WC-Co cemented carbides

J.M. Tarragó, E. Jiménez-Piqué, L. Schneider, D. Casellas, Y. Torres, L. Llanes

Cite this article as: J.M. Tarragó, E. Jiménez-Piqué, L. Schneider, D. Casellas, Y. Torres and L. Llanes, FIB/FESEM experimental and analytical assessment of R-curve behavior of WC-Co cemented carbides, *Materials Science & Engineering A,* http://dx.doi.org/10.1016/j.msea.2015.07.090

This is a PDF file of an unedited manuscript that has been accepted for publication. As a service to our customers we are providing this early version of the manuscript. The manuscript will undergo copyediting, typesetting, and review of the resulting galley proof before it is published in its final citable form. Please note that during the production process errors may be discovered which could affect the content, and all legal disclaimers that apply to the journal pertain.

FIB/FESEM experimental and analytical assessment of

R-curve behavior of WC-Co cemented carbides

J. M. Tarragó[1,2,*], E. Jiménez-Piqué[1,2], L. Schneider[3], D. Casellas[4], Y. Torres[5], L. Llanes[1,2]

[1] CIEFMA, Departament de Ciència dels Materials i Enginyeria Metal·lúrgica, ETSEIB,

Universitat Politècnica de Catalunya, 08028 Barcelona, Spain

[2] CRnE, Centre de Recerca en Nanoenginyeria, Universitat Politècnica de Catalunya,

08028 Barcelona, Spain

[3] Sandvik Hyperion, Coventry CV4 0XG, UK

[4] Fundació CTM Centre Tecnològic, 08243 Manresa, Spain

[5] Departamento de Ingeniería y Ciencia de los Materiales y del Transporte, ETSI,

Universidad de Sevilla, 41092 Sevilla, Spain

ABSTRACT

Exceptional fracture toughness levels exhibited by WC-Co cemented carbides (hardmetals) are due mainly to toughening derived from plastic stretching of crack-bridging ductile enclaves. This takes place due to the development of a multiligament zone at the wake of cracks growing in a stable manner. As a result, hardmetals exhibit crack growth resistance (R-curve) behavior. In this work, the toughening mechanics and mechanisms of these materials are investigated by

* Corresponding author
ETSEIB, Av. Diagonal 647, Barcelona 08028, Spain
+34 934054452
jose.maria.tarrago@upc.edu

combining experimental and analytical approaches. Focused Ion Beam technique (FIB) and Field-Emission Scanning Electron Microscopy (FESEM) are implemented to obtain serial sectioning and imaging of crack-microstructure interaction in cracks arrested after stable extension under monotonic loading. The micrographs obtained provide experimental proof of the developing multiligament zone, including failure micromechanisms within individual bridging ligaments. Analytical assessment of the multiligament zone is then conducted on the basis of experimental information attained from FIB/FESEM images, and a model for the description of R-curve behavior of hardmetals is proposed. It was found that, due to the large stresses supported by the highly constrained and strongly bonded bridging ligaments, WC-Co cemented carbides exhibit quite steep but short R-curve behavior. Relevant strength and reliability attributes exhibited by hardmetals may then be rationalized on the basis of such toughening scenario.

KEYWORDS: A. Micromechanics, FIB/FESEM, R-curve B. Cemented carbides D. Fracture, Toughness

1. INTRODUCTION

WC-Co cemented carbides (hardmetals) are a group of ceramic-metal composite materials with exceptional combinations of strength, toughness and wear resistance. Such remarkable mechanical properties result from the extremely different properties of their two interpenetrating constitutive phases: hard, brittle carbides and a soft, ductile metallic binder (e.g. Refs. [1–3]). As a consequence, they are leading materials in a wide range of extremely demanding applications, where improved tribo-mechanical performance and high reliability are required (e.g. Ref. [4]).

The outstanding fracture toughness levels exhibited by hardmetals are mainly associated with toughening derived from plastic stretching of crack-bridging ductile enclaves [5–7]. Within this context, cracks propagate throughout the composite assembly, leaving isolated metallic ligaments behind the crack tip. As first described by Evans et al. [8], cracks open with increasing applied load, and a multiligament zone develops at the crack wake [9–11]. For WC-Co cemented carbides, this zone is reported to measure about five times the microstructural length scale (carbide grain size) and comprises between 2 and 4 ligaments in the direction of crack propagation [10,11]. The energy required to plastically deform the constrained ductile ligaments is the main contribution to the toughness of these materials [5–12]. Plastic deformation of these reinforcing ligaments is restricted to the binder regions crossed by the crack plane and proceeds through nucleation, growth and coalescence of microcrocavities [6,9–15]. As in the case for brittle solids reinforced with a ductile phase (e.g. Refs. [16–22]), the development of the multiligament zone implies the existence of a rising crack growth resistance (R-curve) behavior in hardmetals [23–27], the size of which is dependent on the width and strength of the ligaments [7,24,28]; and thus, on the microstructural arrangement of the composites under consideration.

R-curve behavior may be described as the ability of a microstructure to develop toughening mechanisms on an advancing crack, which can be done, for example, by screening the crack tip from the far-field driving force [21,29,30]. In the case of ceramics toughened by ductile reinforcements, the magnitude of these stresses increases with crack extension due to the formation of new bridges at the crack wake until a plateau is reached. However, as failure in these materials is intimately related to relatively short cracks (e.g. natural flaws), total development of the multiligament zone may not take place before rupture. In these cases, the crack tip resistance steady-state level, i.e. that corresponding to fracture toughness measured in long cracks, would not be reached [21,25]. Thus, depending on the initial crack size, WC-Co

cemented carbides would be expected to fracture at different crack tip stress intensity factors values (K_R), which are below the long-crack fracture toughness (K_{Ic}) characteristic for each material. On the other hand, R-curve behavior translates into subcritical crack growth of the preexisting flaws, i.e. critical crack size is larger than the initial crack size. It implies a beneficial effect on reducing strength scatter, as compared with that of materials exhibiting a flat R-curve with the same crack tip toughness. Therefore, higher reliability is expected for materials showing rising R-curve characteristics [29,31].

A deep understanding of the fracture process in WC-Co cemented carbides requires a detailed characterization of crack-microstructure interactions. The advent of new and advanced characterization techniques has proven to be extremely helpful for achieving this purpose. Among them, the focused ion beam (FIB) technique has shown to be an adequate technique to evaluate the microstructure and to characterize damage on materials [32–35]. Fruitful examples of its implementation in cemented carbides have been recently reported. They have focused on either characterization of microstructural features (e.g. Refs. [36,37]) or assessment of induced damage (e.g. Refs. [15,38,39]). For these reasons, the aim of this study is to investigate the fracture behavior of WC-Co carbides by documenting and analyzing toughening phenomena through serial FIB sectioning and field emission scanning electron microscopy (FESEM) imaging. In doing so, crack-microstructure interactions are quantified, and an analytical model for the description of R-curve behavior of hardmetals is then proposed.

2. MATERIALS AND EXPERIMENTAL ASPECTS

The investigated material is a medium grain sized WC-11$_{\%Wt.}$Co (**Figure 1**) supplied by Sandvik Hyperion. Microstructural characteristics, including binder content (%$_{Wt.}$ binder), mean grain size (d_{WC}), carbide contiguity (C_{WC}), and binder mean free path (λ_{binder}), are listed in **Table 1**.

Mean grain size was measured following the linear intercept method [40], using FESEM micrographs taken in a JEOL-7001F unit. Carbide contiguity was deduced from best-fit equations following empirical relationships given by Roebuck and Almond [2], but extending them to include carbide size influence on the basis of extensive analysis of data from open literature [41]. Binder mean free path was finally estimated from the carbide contiguity data [1,2].The hardmetal grade under consideration exhibited a Vickers hardness of 12.8 ± 0.2 GPa. This value was averaged over five measurements made under an applied force of 294N.
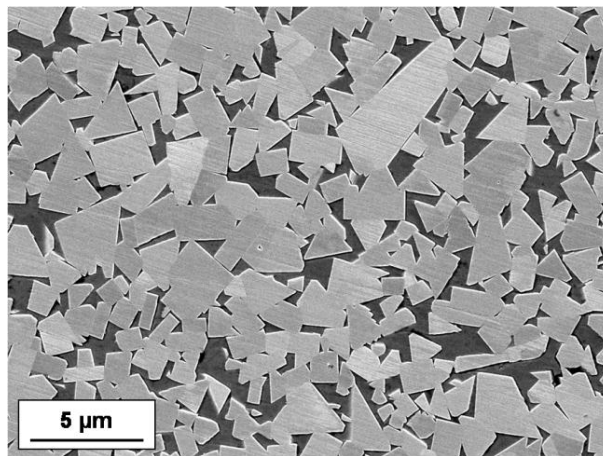

Figure 1. FESEM micrograph corresponding to the microstructure of the hardmetal grade studied.

Assessment of toughening mechanics and mechanisms was the main experimental activity in this investigation. Within this context, plane strain fracture toughness (K_{Ic}) evaluation and corresponding fractographic examination of broken specimens were first conducted. K_{Ic} was determined using 45x10x5 mm single edge pre-cracked notch beam specimens with a pre-crack length-to-specimen width ratio of about 0.5, following the procedure reported by Llanes and coworkers [27,42]. Five specimens were tested, yielding an average fracture toughness of 13.9 ± 0.3 MPa·m$^{1/2}$. Fractographic analysis was carried out by means of FESEM in order to discern fracture mechanisms within constitutive phases.

Binder content	d_{WC} (µm)	C_{wc}	λ_{Co} (µm)
$11_{\%Wt.}$ Co	1.12 ± 0.71	0.38 ± 0.07	0.42 ± 0.28

Table 1. Microstructural parameters for the investigated material.

The mechanical/fractography characterization was followed by a detailed study of crack-microstructure interactions under monotonic loading. It was done by means of serial sectioning and imaging using a FIB/FESEM (Zeiss Neon 40) equipment. However, assessment of toughening associated with R-curve behavior development requires analysis of stably grown and arrested cracks under increasing monotonic loading, a rather challenging scenario for materials like WC-Co cemented carbides, which are known to have a brittle behavior. With this purpose, four Vickers indentations were produced (under 490 N applied load) at the centre of the studied specimens (4 mm x 3 mm x 45 mm) with a span of 2 mm between them. Prior to indentation tests the surface which was later indented and subjected to tensile bending loads was polished to mirror-like finish and the corners were rounded to reduce their stress raiser effect. Care was taken to orient one set of the corresponding Palmqvist cracks of each indentation flaw parallel to the cross section of the specimen where the prospective rupture would occur. The initial length of such cracks was comprised between 25-35 µm. Residual stresses due to indentation for all the controlled flaws were relieved by subjecting the specimens to cyclic tensile bending (load ratio of 0.1 and frequency 10 Hz) in order to induce stable (fatigue) crack growth. In doing so, more than 50000 bending cycles were applied and the cracks extended about 30-60 µm. Finally, fracture of cracked specimens was induced in flexure (four-point bending with outer and inner spans of 40 and 20 mm, respectively) by applying a loading rate of 100 N/s. The sample fractured by the propagation of one indentation induced crack, but those corresponding to the remaining indentations extended and arrested before failure. Therefore, several surviving cracks of variable lengths were obtained for subsequent FIB serial sectioning

process (**Figure 2a**). Concretely, the selected crack for the sectioning and imaging process had a final length of approximately 90μm from the indentation corner.
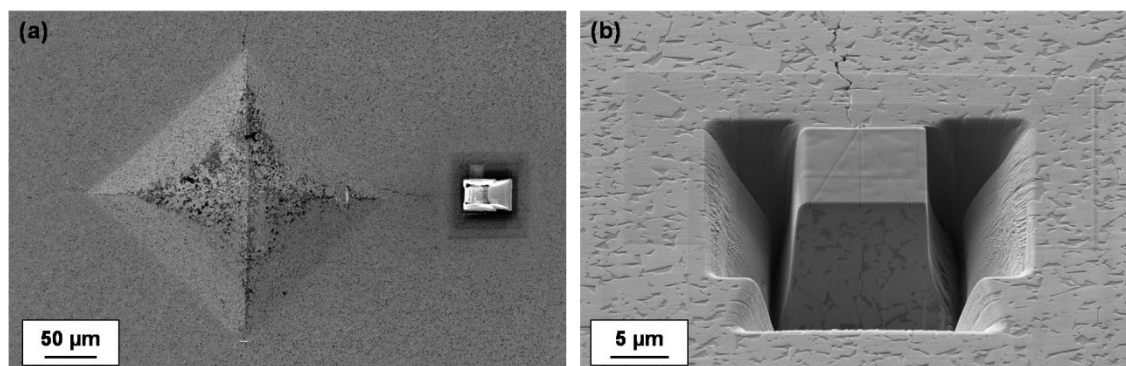

Figure 2. FESEM micrographs corresponding to: (a) deposited Pt layer and FIB-milled trench at region close to the tip of a crack arrested after stable growth, and (b) U-trench generated by FIB around the region of interest.

Combined FIB/FESEM serial sectioning and imaging processes were conducted in a region close to the crack tip corresponding to a fissure propagated under monotonic loads and arrested before failure. Before ion milling, a platinum thin protective layer was deposited on the area of interest in order to reduce curtain effects on the subsequent milling cuts. A U-shaped trench with one cross-sectional surface (perpendicular to the crack path and to the specimen surface) was produced by FIB (**Figure 2b**). Then, a series of images of crack-microstructure interaction was obtained by periodic removal of the material by selectively bombarding the material with Ga^+ ions, within the U-shaped crater parallel to the cross-sectional surface (e.g. **Figure 3**). For that purpose, FIB was selected to operate at a voltage of 30 kV and at a current intensity of 10 pA. On the other hand, FESEM gun operated at 2 kV. More than 600 images (15 μm × 15 μm) were recorded with a 20 nm span between them.
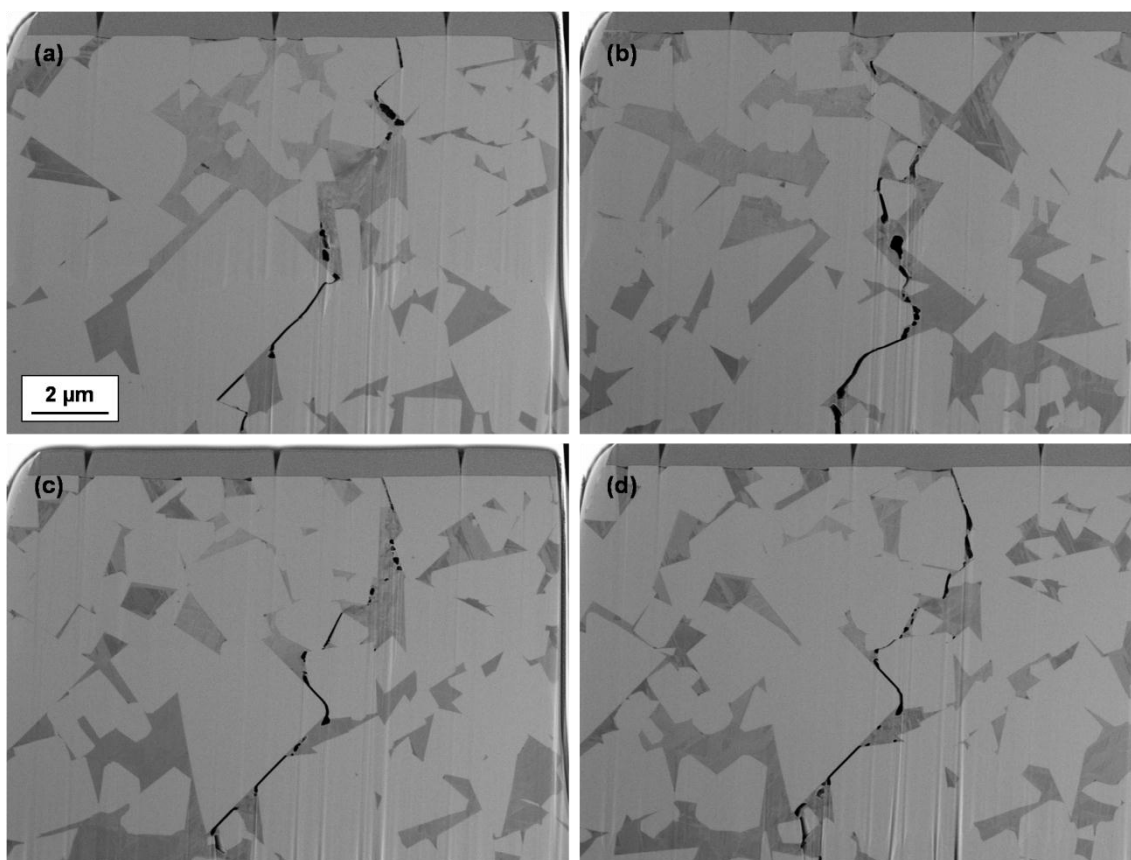
Figure 3. FESEM micrographs corresponding to crack-microstructure interactions, as imaged on serial sections obtained by means of FIB tomography.

3. RESULTS AND DISCUSSION

3.1. Toughening mechanisms in WC-Co cemented carbides

In agreement with previous findings reported in the literature (e.g. Refs. [10,12,43]), fracture surfaces corresponding to cracks propagated under monotonic loading exhibit well-defined dimples within the binder (**Figure 4a**), suggesting a purely ductile fracture mechanism. Thus, aiming to document, understand and evaluate the crack growth process under monotonic loading, transversal cut FIB/FESEM images corresponding to the bridging process zone at the crack wake were analyzed. These micrographs clearly point out to the nucleation, growth and coalescence of microvoids as the main failure mechanism of binder ligaments in the crack path

(**Figure 4b**). An example of such damage evolution within a binder ligament is shown in **Figure 5**. Obtained micrographs represent experimental evidence (and thus validate) several statements postulated by Sigl and co-workers after their systematic and thorough investigation on the fracture behavior of WC-Co cemented carbides [6,10,11,13], as follows:

(1) The crack initially propagates through the composite assembly, leaving binder ligaments at the crack wake acting as bridges which hinder the crack from propagating further (e.g. **Figures 3a and 3d**).

(2) Ductile enclaves elongate during crack opening. This deformation is compensated by the formation of microcavities inside the ligament to uphold volume constancy [10,11]. Then, localized plastic deformation occurs at the bridges between the voids, leading to final failure of the ligaments by growth and coalescence of the microcavities (**Figure 5**).

(3) Voids tend to nucleate at carbide corners (stress raisers) (e.g. **Figure 3b**) and close to carbide-binder interfaces (but within the binder) (e.g. **Figure 3c**), where high triaxial stresses are reached [13]. Voids that run close and parallel to binder-carbide interfaces are smaller but higher in number than the voids that nucleate in binder regions more distant to interfaces, as can be appreciated in **Figures 3 and 4a**. It has also been observed that the mean depth of the plastic zone is always smaller than the mean free path in the binder and no metal/ceramic debonding has been found.
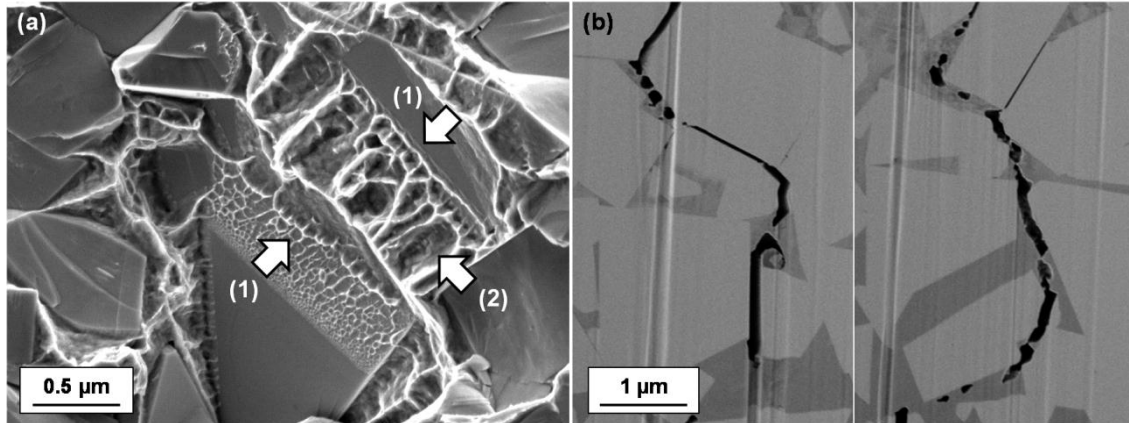
Figure 4. FESEM micrographs corresponding to (a) crack growth micromechanisms within the binder in the fracture surface, and (b) experimental evidence (FIB/FESEM image) of dimple formation within the binder following nucleation, growth and coalescence of microvoids. Please note that the arrows marked with (1) indicate the formation of dimples from voids that run close to the interface, while those marked with (2) refers to the formation of larger dimples in binder regions more distant to interfaces.

In summary, the existence of multiligament zones as primary foundations for the outstanding fracture toughness of hardmetals is validated. Additionally, the existence of such crack wake bridging mechanism can be directly related to the R-curve behavior of WC-Co cemented carbides. Within this context, the interpenetrating two-phase composite microstructure plays a critical role in defining effective toughness, R-curve characteristics, reliability and damage tolerance.
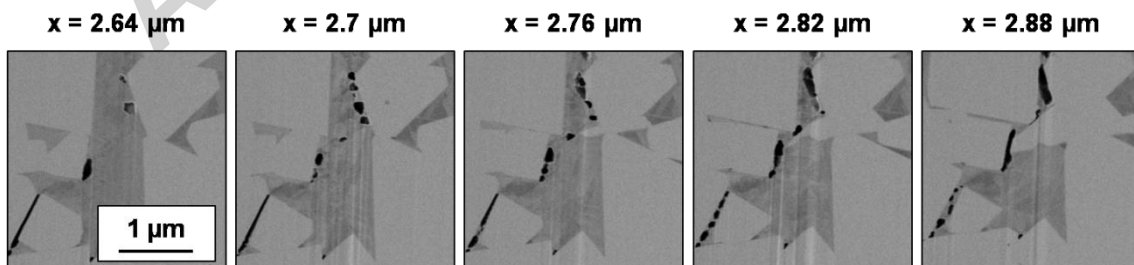

Figure 5. Series of FESEM micrographs outlining the multiligament zone at the crack wake for hardmetals. These micrographs evidence damage evolution within a binder ligament as the

distance from the crack tip (x) increases for a crack propagated (stable growth) under monotonic loading.

3.2. Analytical assessment of R-curve behavior: toughening mechanics

In this section the estimation of the R-curve behavior of the investigated hardmetal is attempted through the analysis of a series of images of crack-microstructure interaction, and the implementation of analytical models for describing the behavior of metal reinforced ceramics.

The contribution of the constrained ductile reinforcements to fracture toughness (ΔG_c) can be related to the nominal stress of the ligaments for a given crack-opening displacement (u) according to [7,31]:

$$\Delta G_c = A_f \int_0^{u^*} \sigma(u)du = A_f W = D^* A_f \sigma_y \left(\frac{\lambda_{Co}}{2}\right) \qquad (1)$$

where A_f is the area-fraction of ductile material intersected by the crack-plane, u^* is the crack opening at the point when the ductile ligament fails, σ is the normal stress on the bridge, σ_y is the yield strength of the initially unconstrained binder, λ_{Co} is the binder mean free path, and W is a measure of the toughening capacity of a given ductile reinforcement. D^* is a "work of rupture" function that depends on the constraint and the constitutive properties of the binder [7,27,44], and on the interface strength. Thus, the effective toughness of bridged ceramics can be written in terms of the crack tip stress intensity factor (K_R) as [7,27,31]:

$$K_R = \sqrt{K_t{}^2 + \frac{D^* E A_f \sigma_0 \left(\frac{\lambda_{Co}}{2}\right)}{(1-v^2)}} \qquad (2)$$

where K_t is the critical crack tip stress intensity factor required for crack initiation, and E and
are the Young's modulus and the Poisson ratio of the composite, respectively.

Through the analysis of imaged transversal micrographs, the R-curve of the studied WC-Co
cemented carbide may be estimated according to expression (2). In this regard, and on the basis
of obtained FESEM/FIB images, crack opening displacement (u) can be experimentally
measured as a function of the distance from the crack tip (x). These results are shown in **Figure
6**. With this purpose, FESEM transversal micrographs were binarized such that the cracks were
represented in black and the other phases in white. Then, the geometry of the crack chords was
analyzed and its area (S) and maximum length (L) determined. Crack opening distance values
were subsequently estimated by considering the crack chords as rectangles of area $S_i = L_i u_i$. In
the few cases where the curtaining effect affected the geometry and size of the chords, the
images were manually corrected to avoid a disruption of the results. Free available Fiji software
was used for this analysis. An interval of 400 nm between analyzed FESEM images was
selected, and more than 30 micrographs were processed. Nevertheless, the first obtained
micrograph did not correspond to the crack tip but rather to a position few microns behind.
Hence, distance from the first analyzed transversal FESEM micrograph to the crack tip was
approximated by the measuring crack opening displacement at this point, and comparing it to
the one theoretically deduced for an un-bridged material using the Irwin Parabola [45] of
equation:

$$u(x) = \frac{K_{Ic}}{E/(1-v^2)} \left(\frac{8x}{\pi}\right)^{1/2} \qquad (3)$$

It is interesting to note that, although crack-opening displacement curve follows a similar trend to that described by Irwin Parabola, it is slightly shifted down. A plausible reason for this relative displacement may be the presence of bridging ligaments that exert closure stresses on the crack wake, as reported for other ceramic-metal composites [19]. The first stage of the *u-x* curve follows a power law dependence of equation:

$$u(x) = mx^n \qquad (4)$$

where *m* and *n* are constants. In the case of the studied hardmetal, a best-fit of experimental data yields values of 0.0397 and 0.415 for the referred constants, respectively. Nevertheless, at a distance of approximately 10 μm behind the crack tip, this toughening mechanism is no longer effective and *u* values increase much faster.
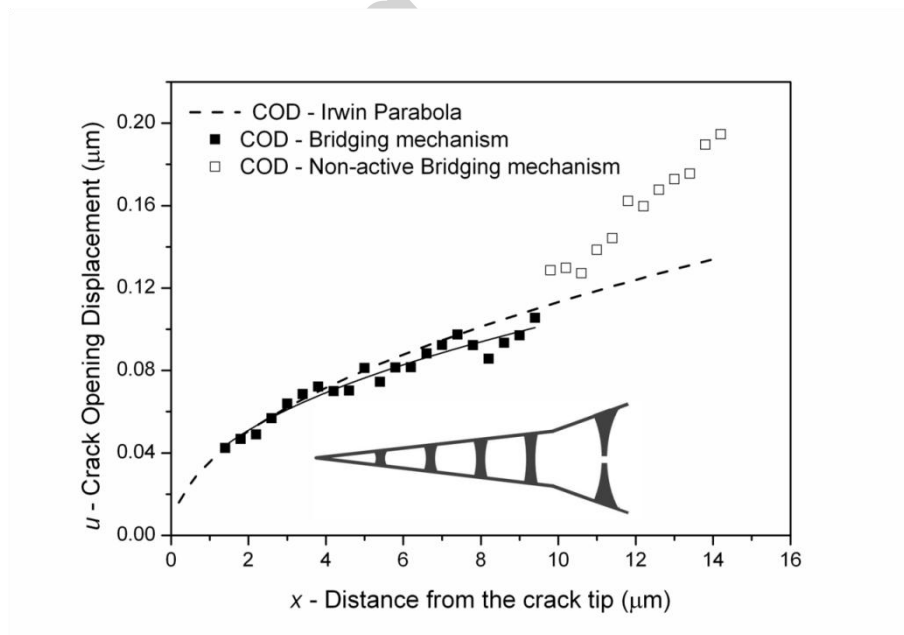
Figure 6. Evolution of the crack opening displacement as a function of the distance from the crack tip. Experimental results are compared to the Irwin parabola [45] for un-bridged materials. A schematic representation of the crack tip bridging process is also included.

From the recorded series of FIB/FESEM images, the area-fraction of ductile material intersected by the crack-plane (A_f) has also been measured, and results are plotted in **Figure 7**. In this case the measurements were performed manually. It is interesting to remark that once again, a change in tendency is observed at a distance of about 10 μm from the crack tip. Initially the percentage of fractured binder remains stable at values between 40-60%, but as ligaments cease being effective, A_f values increase linearly until ligaments fracture entirely.
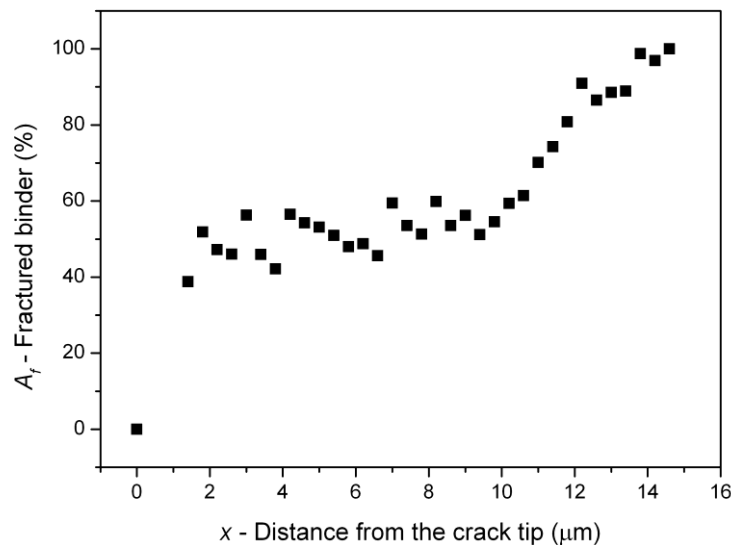

Figure 7. Percentage of fractured binder in the crack path as a function of the distance from the crack tip as obtained by inspection of the FIB sequential images.

Following the above findings, a multiligament zone may then be considered to be fully developed (i.e. plateau in the R-curve is reached) once a 60% of the ligaments are fractured. Such experimentally assessed information can then be combined with the known

microstructural parameters and mechanical properties of the studied WC-Co cemented carbide for estimating its "work of rupture" according to expression (1). As referred above, D* depends on the constraint level as well as on the properties of both interface and reinforcing ligaments. D* may assume values from 0.75 for complete bonding between phases up to 8 for limited debonding and fracture of the brittle phase [7,24,46,47]. Assessment of D* from equation (2) requires reliable inputs for yield strength of unconstrained binder ligaments (σ_0) and critical crack tip stress intensity factor required for crack initiation (K_t). A value of 600 MPa may be taken for σ_0, from the reference work by Roebuck and Almond [48]. This value of strength is significantly higher than that expected for bulk Co, as expected from the solid solution strengthening contribution associated with dissolved tungsten and carbon [48,49]. It may be assumed that the K_t value is equal to the corresponding fatigue crack growth threshold (for a load ratio of 0.1), which in its turn is linearly dependent on the grain size [50] due to the action of crack-deflection as an additional toughening mechanism in cemented carbides [27,50]. Under these assumptions, equation (2) yields a value for D* of 2.8, in satisfactory agreement with previous estimations reported in medium- and coarse-grained WC-Co cemented carbides [27].

Several authors (e.g. Refs. [51,52]) have proposed and validated a function for representing bridging stress in toughened ceramics as a function of the distance from crack tip with the form:

$$\sigma(x) = \alpha x^2 - \beta x^3 \qquad (5)$$

where α and β are arbitrary constants. Then, by combining expressions (4) and (5), bridging stress can be written as a function of u as follows:

$$\sigma(u) = \alpha m^2 u^{2n} - \beta m^3 u^{3n} \quad (6)$$

The α and β constants can be determined by solving equation (6) for specific boundary conditions. On one hand, it is known that $\sigma(u)$ equals zero when the ductile material fails (i.e. $u = u^*$). On the other hand, from expression (3) it is known that:

$$\int_0^{u^*} \sigma(u) du = D^* \sigma_0 \left(\frac{\lambda_{Co}}{2} \right) \quad (7)$$

By solving both equations numerically, α and β can be determined and the σ-μ curve for the binder bridges drawn (**Figure 8**). In accordance with previous investigations [6,11,53], strength values up to 8 times higher than the ones expected for the unconstrained Co-alloy were obtained. In the curve plotted in **Figure 8**, the first region is dominated by an elastic-bridging mechanism leading to a fast rise of bridging stress [24]. It reaches a maximum value at u about 30 nm. Subsequently, plastic deformation of bridges proceeds by necking. It results in an effective bridging stress decrease, even though ductile enclaves experience work hardening as deformation takes place [6,7,24,28].
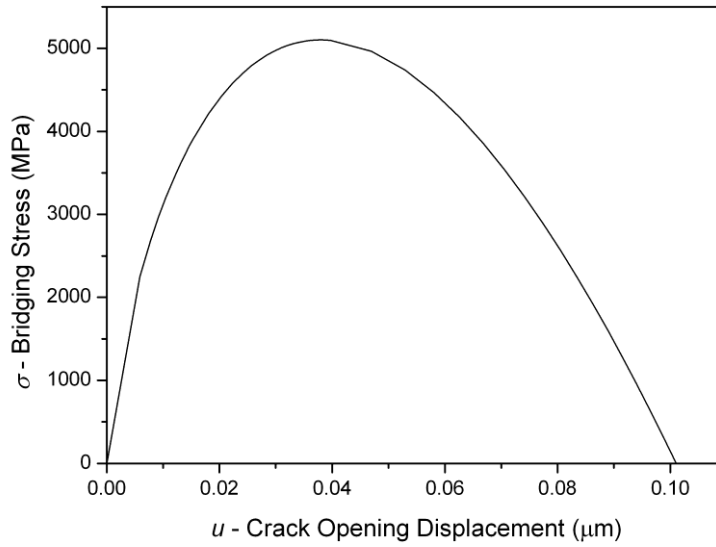
Figure 8. Bridging stress distribution as a function of the crack opening displacement as calculated from expressions (6) and (7).

Once the dependence of bridging stress on crack-opening displacement is known, value of D* for a given *u* may be deduced using equation (7). This enables the estimation of the R-curve for the investigated WC-Co cemented carbide on the basis of equation (1), and results are shown in **Figure 9**. A good correlation ($R^2 = 0.94$) is obtained between estimated data and equation proposed by Ramachandran and Shetty for describing R-curve response [54]:

$$K_R = K_{Ic} - (K_{Ic} - K_t) \, exp \left[-\frac{x}{t} \right] \qquad (8)$$

where *t* is a normalizing crack length parameter. The fitting curve yields values for K_{Ic}, K_t and *t* of 13.7 MPa·m$^{1/2}$, 7.5 MPa·m$^{1/2}$ and 3.5, respectively. The first two values are quite close to those experimentally determined for plane-strain fracture toughness (K_{Ic} = 13.9 MPa·m$^{1/2}$) and

fatigue crack growth threshold ($K_t = 7.2$ MPa·m$^{1/2}$) values for the investigated cemented carbide [50] while the t parameter is related to the microstructural size of the hardmetal under consideration.
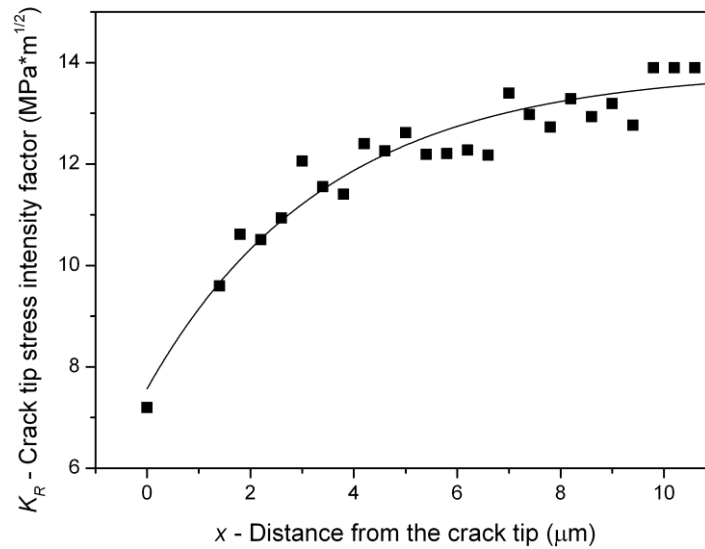

Figure 9. Estimated R-curve behavior for the investigated cemented carbide. Black points correspond to the estimated K_R values according to equation (2), while the black line is obtained after a best-fitting of such points according to equation (8), proposed by Ramachandran and Shetty [54] for describing R-curve response of ceramic/metal materials.

A critical appraisal of this curve permits highlighting two interesting facts. First, cemented carbides exhibit a pronounced R-curve behavior, due to the development of a toughening-effective multiligament zone behind the crack tip. Within this context, R-curve shape can be described as short in length but exhibiting a steep slope, due to the extremely large bridging stresses developed by the strong and tightly bonded constrained ligaments [6,11]. Regarding extension of this multiligament zone, it was found to be about 6-7 times the microstructural length scale of hardmetals ($[d_{WC} + \lambda_{binder}]$), comprising then between 4 and 6 bridging ligaments. These experimental and analytical findings are in complete agreement with those stated in the investigation conducted by Sigl and coworkers [10,11]. Second, the first few microns of the

multiligament zone account for most of the crack tip shielding effect. In this regard, at 2 μm from the crack tip almost half of the effective action of the binder bridges has already been developed. Moreover, this shielding effectiveness percentage increases up to 75% at a crack tip distance of 4 μm.

It should be emphasized that catastrophic failure of WC-Co cemented carbides is related to the propagation of pre-existing flaws, either inherent to the manufacturing process (e.g. Refs. [2,55]) or induced under service conditions (e.g. Refs. [39,56,57]), and its strength is intimately associated with nature, size and geometry of such defects [2]. In this regard, one beneficial aspect of materials exhibiting R-curve behavior is that effective toughness level rises as the size of the flaw also increases [21]. As a consequence, the existence of R-curve behavior is expected to impart in-service reliability and enhanced damage tolerance to the corresponding structural components [31]. From this structural viewpoint, to delve deeper into the knowledge of R-curve characteristics of cemented carbides becomes relevant not only for development of new and improved microstructural combinations, but also for proper material selection aiming to optimize performance in extremely demanding applications. Within this context, the results of this study postulate and validate the implementation of combined FIB/FESEM experimental and analytical approaches for assessing the microstructural influence on effective toughness under service conditions (on the basis of R-curve behavior) for these materials.

4. CONCLUSIONS

In this study, toughening mechanics and mechanisms of WC-Co cemented carbides were studied. The investigation was done by combining experimental and analytical assessment of R-curve behavior in a given hardmetal grade. The experimental work includes serial FIB/FESEM sectioning and imaging of crack-microstructure interaction within the bridging process zone at

the crack wake. Based on the main findings of the study, the following conclusions may be drawn:

1. Unequivocal proof of the multiligament zone as the foundation for understanding toughness and R-curve behavior in hardmetals is provided. Binder bridges at the crack wake are the main toughening mechanism in cemented carbides, and fail by nucleation, growth and coalescence of microcavities. These microvoids tend to nucleate within the binder but close to either carbide corners or carbide-binder interfaces, where high triaxiality stress and strain conditions are fulfilled. It was found that the size of the multiligament zone extends about 6-7 times the microstructural length scale of the hardmetal studied, comprising then between 4 and 6 bridging ligaments.

2. The crack opening displacement (u) has been experimentally measured as a function of the distance from the crack tip. While bridging stresses are active, u values increase following a power law dependence. However, as ductile ligaments cease being active, u values increase at higher rates with respect to the distance from the crack tip.

3. An analytical representation of the evolution of bridging stress as a function of crack opening displacement was presented. In accordance with previous investigations, bridging ligaments exhibit strength levels much higher than the ones expected for an unconstrained Co-alloy.

4. R-curve behavior for the WC-Co cemented carbide studied is assessed by critical analysis of series of FIB/FESEM images of crack-microstructure interaction at the wake of stably grown cracks. As a result, cemented carbides are found to exhibit a steep but short R-curve behavior, due to the large stresses supported by the highly constrained

and strongly bonded bridging ligaments. Thus, relevant strength and reliability attributes exhibited by hardmetals may be rationalized on the basis of this toughening scenario.

ACKNOWLEDGEMENTS

REFERENCES

[1]   H.E. Exner, Physical and chemical nature of cemented carbides, Int. Met. Rev. 24 (1979) 149–173.

[2]   B. Roebuck, E.A. Almond, Deformation and fracture processes and the physical metallurgy of WC-Co hardmetals, Int. Mater. Rev. 33 (1988) 90–110.

[3]   A.V. Shatov, S.S. Ponomarev, S.A. Firstov, Fracture and strength of hardmetals at room temperature, in: V.K. Sarin, D. Mari, L. Llanes (Eds.), Comprehensive Hard Materials, Elsevier, 2014: pp. 301–343.

[4]   L.J. Prakash, Fundamentals and general applications of hardmetals, in: V.K. Sarin, D. Mari, L. Llanes (Eds.), Comprehensive Hard Materials, Elsevier, 2014: pp. 29–90.

[5]   A.G. Evans, R.M. McMeeking, On the toughening of ceramics by strong reinforcements, Acta Metall. 34 (1986) 2435–2441.

[6]   L.S. Sigl, P.A. Mataga, B.J. Dalgleish, R.M. McMeeking, A.G. Evans, On the toughness of brittle materials reinforced with a ductile phase, Acta Metall. 36 (1988) 945–953.

[7]   M.F. Ashby, F.J. Blunt, M. Bannister, Flow characteriztics of highly constrained metal wires, Acta Metall. 37 (1989) 1847–1857.

[8]   A.G. Evans, A.H. Heuer, D.L. Porter, The fracture toughness of ceramics, in: D.M.R. Taplin (Ed.), Proceedings of the 4th International Conference on Fracture, Pergamon, Waterloo, 1977: pp. 529–556.

[9]   V.D. Krstic, On the fracture of brittle-matrix/ductile-particle composites, Philos. Mag. A 48 (1983) 695–708.

[10] L.S. Sigl, H.E. Exner, Experimental study of the mechanics of fracture in WC-Co alloys, Metall. Trans. A 18A (1987) 1299–1308.

[11] L.S. Sigl, H.F. Fischmeister, On the fracture toughness of cemented carbides, Acta Metall. 36 (1988) 887–897.

[12] R.K. Viswanadham, T.S. Sun, E.F. Drake, J. Peck, Quantitative fractography of WC-Co cermets by Auger spectroscopy, J. Mater. Sci. 16 (1981) 1029–1038.

[13] H.F. Fischmeister, S. Schmauder, L.S. Sigl, Finite element modelling of crack propagation in WC- Co hard metals, Mater. Sci. Eng. A 105/106 (1988) 305–311.

[14] C. McVeigh, W.K. Liu, Multiresolution modeling of ductile reinforced brittle composites, J. Mech. Phys. Solids. 57 (2009) 244–267.

[15] J.M. Tarragó, E. Jimenez-Piqué, M. Turón-Viñas, L. Rivero, I. Al-Dawery, L. Schneider, L. Llanes, Fracture and fatigue behavior of cemented carbides: 3D focused ion beam tomography of crack-microstructure interactions, Int. J. Powder Metall. 50 (2014) 1–10.

[16] L. Murugesh, K.T. Venkateswara Rao, R.O. Ritchie, Powder processing of ductile-phase-toughened Nb-Nb$_3$Al in situ composites, Mater. Sci. Eng. A 189 (1994) 201–208.

[17] D.R. Bloyer, K.T. Venkateswara Rao, R.O. Ritchie, Resistance-curve toughening in ductile/brittle layered structures: Behavior in Nb/Nb$_3$Al laminates, Mater. Sci. Eng. A 216 (1996) 80–90.

[18] Y. Kagawa, K. Sekine, Toughening by continuous single fiber bridging in ceramic matrix composite, Mater. Sci. Eng. A 221 (1996) 163–172.

[19] O. Raddatz, G.A. Schneider, N. Claussen, Modelling of R-curve behavior in ceramic/metal composites, Acta Metall. 46 (1998) 6381–6395.

[20] O. Sbaizero, S. Roitti, G. Pezzotti, R-curve behavior of alumina toughened with molybdenum and zirconia particles, Mater. Sci. Eng. A 359 (2003) 297–302.

[21] D. Munz, What can we learn from R-curve measurements?, J. Am. Ceram. Soc. 90 (2007) 1–15.

[22] Y.L. Xue, S.M. Li, H. Zhong, H.Z. Fu, Characterization of fracture toughness and toughening mechanisms in Laves phase Cr$_2$Nb based alloys, Mater. Sci. Eng. A 638 (2015) 340–347.

[23] H.G. Schmid, The mechanisms of fracture of WC-11wt%Co between 20°C and 1000°C, Mater. Forum. 10 (1987) 184–197.

[24] P.A. Mataga, Deformation of crack-bridging ductile reinforcements in toughened brittle materials, Acta Metall. 37 (1989) 3349–3359.

[25] Y. Torres, D. Casellas, M. Anglada, L. Llanes, Fracture behavior of hardmetals: Implementation of flaw configuration modeling and R-curve concepts, in: H. Danninger, R. Ratzi (Eds.), Proceedings Euro PM 2004, EPMA, Vienna, Austria, 2004: pp. 551-556.

[26] Y. Torres, R. Bermejo, L. Llanes, M. Anglada, Influence of notch radius and R-curve behaviour on the fracture toughness evaluation of WC–Co cemented carbides, Eng. Fract. Mech. 75 (2008) 4422–4430.

[27] Y. Torres, J.M. Tarrago, D. Coureaux, E. Tarrés, B. Roebuck, P. Chan, M. James, B. Liang, M. Tillman, R.K. Viswanadham, K.P. Mingard, A. Mestra, L. Llanes, Fracture and fatigue of rock bit cemented carbides: Mechanics and mechanisms of crack growth resistance under monotonic and cyclic loading, Int. J. Refract. Met. Hard Mater. 45 (2014) 179–188.

[28] G.R. Odette, B.L. Chao, J.W. Sheckherd, G.E. Lucas, Ductile phase toughening mechanisms in a TiAl-TiNb laminate composite, Acta Metall. Mater. 40 (1992) 2381–2389.

[29] R.O. Ritchie, K.J. Koester, S. Ionova, W. Yao, N.E. Lane, J.W. Ager, Measurement of the toughness of bone: a tutorial with special reference to small animal studies, Bone 43 (2008) 798–812.

[30] M.E. Launey, R.O. Ritchie, On the fracture toughness of advanced materials, Adv. Mater. 21 (2009) 2103–2110.

[31] A.G. Evans, Perspective on the development of high-toughness ceramics, J. Am. Ceram. Soc. 73 (1990) 187–206.

[32] J.M. Cairney, P.R. Munroe, J.H. Schneibel, Examination of fracture surfaces using focused ion beam milling, Scr. Mater. 42 (2000) 473–478.

[33] B. Inkson, M. Mulvihill, G. Möbus, 3D determination of grain shape in a FeAl-based nanocomposite by 3D FIB tomography, Scr. Mater. 45 (2001) 753–758.

[34] B. Inkson, T. Steer, G. Möbus, T. Wagner, Subsurface nanoindentation deformation of Cu–Al multilayers mapped in 3D by focused ion beam microscopy, J. Microsc. 201 (2001) 256–269.

[35] Z.-H. Xie, P.R. Munroe, R.J. Moon, M. Hoffman, Characterization of surface contact-induced fracture in ceramics using a focused ion beam miller, Wear 255 (2003) 651–656.

[36] K.P. Mingard, H.G. Jones, M.G. Gee, B. Roebuck, A. Gholinia, B. Winiarski, P. Whiters, 3D imaging of structures in bulk and surface modified WC-Co hardmetals, in: Proceedings Euro PM 2012, EPMA, Basel, 2012: pp. 155–160.

[37] I. Borgh, P. Hedström, J. Odqvist, A. Borgenstam, J. Ågren, A. Gholinia, B. Winiarski, P.J. Withers, G.E. Thompson, K. Mingard, M.G. Gee, On the three-dimensional structure of WC grains in cemented carbides, Acta Mater. 61 (2013) 4726–4733.

[38] A.J. Gant, M.G. Gee, D.D. Gohil, H.G. Jones, L.P. Orkney, Use of FIB/SEM to assess the tribo-corrosion of WC/Co hardmetals in model single point abrasion experiments, Tribol. Int. 68 (2013) 56–66.

[39] J.M. Tarragó, G. Fargas, E. Jimenez-Piqué, A. Felip, L. Isern, D. Coureaux, J.J. Roa, I. Al-Dawery, J. Fair, L. Llanes, Corrosion damage in WC–Co cemented carbides: residual strength assessment and 3D FIB-FESEM tomography characterisation, Powder Metall. 57 (2014) 324–330.

[40] ISO 4499-2:2008 Hardmetals. Metallographic determination of microstructure. Part 2: Measurement of WC grain size, Geneva, 2008.

[41] D. Coureaux, Comportamiento mecánico de carburos cementados WC-Co: Influencia de la microestructura en la resistencia a la fractura, la sensibilidad a la fatiga y la tolerancia al daño inducido bajo solicitaciones de contacto, PhD Thesis, Universitat Politècnica de Catalunya, 2012.

[42] Y. Torres, D. Casellas, M. Anglada, L. Llanes, Fracture toughness evaluation of hardmetals: influence of testing procedure, Int. J. Refract. Met. Hard Mater. 19 (2001) 27–34.

[43] G. Erling, S. Kursawe, S. Luyck, H.G. Sockel, Stable and unstable fracture surface features in WC-Co, J. Mater. Sci. Lett. 19 (2000) 437–438.

[44] J. Riesch, J.-Y. Buffiere, T. Höschen, M. di Michiel, M. Scheel, C. Linsmeier, J.-H. You, In situ synchrotron tomography estimation of toughening effect by semi-ductile fibre reinforcement in a tungsten-fibre-reinforced tungsten composite system, Acta Mater. 61 (2013) 7060–7071.

[45] G.R. Irwin, Fracture, in: Handbook Der Physics, Springer-Verlag, Berlin, 1958.

[46] H.C. Cao, B.J. Dalgleish, H.E. Dève, C. Elliott, A.G. Evans, R. Mehrabian, G.R. Odette, A test procedure for characterizing the toughening of brittle intermetallics by ductile reinforcements, Acta Metall. 37 (1989) 2969–2977.

[47] H.E. Dève, A.G. Evans, G.R. Odette, R. Mehrabian, M.L. Emiliani, R.J. Hecht, Ductile reinforcement toughening of γ-TiAl: Effects of debonding and ductility, Acta Metall. Mater. 38 (1990) 1491–1502.

[48] B. Roebuck, E.A. Almond, The influence of composition, phase transformation and varying the relative F.C.C. and H.C.P. phase contents on the properties of dilute Co-W-C Alloys, Mater. Sci. Eng. 66 (1984) 179–194.

[49] J.J. Roa, E. Jiménez-Piqué, J.M. Tarragó, M. Zivcec, C. Broeckmann, L. Llanes, Berkovich nanoindentation and deformation mechanisms in a hardmetal binder-like cobalt alloy, Mater. Sci. Eng. A 621 (2015) 128–132.

[50]   J.M. Tarragó, J.J. Roa, V. Valle, J.M. Marshall, L. Llanes, Fracture and fatigue behavior of WC–Co and WC–CoNi cemented carbides, Int. J. Refract. Met. Hard Mater. 49 (2015) 184–191.

[51]   S.R. Choi, J.A. Salem, A.S. William, Estimation of crack closure stresses for in situ toughened silicon nitride with 8 wt% scandia, J. Am. Ceram. Soc. 75 (1992) 1508–1511.

[52]   G. Pezzotti, H. Huebner, H. Suenobu, S. Orfeo, T. Nishida, Analysis of near-tip crack bridging in WC/Co cermet, J. Eur. Ceram. Soc. 19 (1999) 119–123.

[53]   M.H. Poech, H.F. Fischmeister, Deformation of two-phase materials: A model based on strain compatibility, Acta Metall. Mater. 40 (1992) 487–494.

[54]   N. Ramachandran, D.K. Shetty, Rising crack growth resistance (R-Curve) behavior of toughened alumina and silicon nitride, J. Am. Ceram. Soc. 74 (1991) 2634–2641.

[55]   B. Casas, Y. Torres, L. Llanes, Fracture and fatigue behavior of electrical-discharge machined cemented carbides, Int. J. Refract. Met. Hard Mater. 24 (2006) 162–167.

[56]   V.A. Pugsley, G. Korn, S. Luyckx, H.G. Sockel, W. Heinrich, M. Wolf, H. Feld, R. Schulte, The influence of a corrosive wood-cutting environment on the mechanical properties of hardmetal tools, Int. J. Refract. Met. Hard Mater. 19 (2001) 311–318.

[57]   A. Góez, D. Coureaux, A. Ingebrand, B. Reig, E. Tarrés, A. Mestra, A. Mateo, E. Jiménez-Piqué, L. Llanes, Contact damage and residual strength in hardmetals, Int. J. Refract. Met. Hard Mater. 30 (2012) 121–127.

LIST OF FIGURES

Figure 1. FESEM micrograph corresponding to the microstructure of the hardmetal grade studied.

Figure 2. FESEM micrographs corresponding to: (a) deposited Pt layer and FIB-milled trench at region close to the tip of a crack arrested after stable growth, and (b) U-trench generated by FIB around the region of interest.

Figure 3. FESEM micrographs corresponding to crack-microstructure interactions, as imaged on serial sections obtained by means of FIB tomography.

Figure 4. FESEM micrographs corresponding to (a) crack growth micromechanisms within the binder in the fracture surface, and (b) experimental evidence (FIB/FESEM image) of dimple formation within the binder following nucleation, growth and coalescence of microvoids. Please note that the arrows marked with (1) indicate the formation of dimples from voids that run close

to the interface, while those marked with (2) refers to the formation of larger dimples in binder regions more distant to interfaces.

Figure 5. Series of FESEM micrographs outlining the multiligament zone at the crack wake for hardmetals. These micrographs evidence damage evolution within a binder ligament as the distance from the crack tip (x) increases for a crack propagated (stable growth) under monotonic loading.

Figure 6. Evolution of the crack opening displacement as a function of the distance from the crack tip. Experimental results are compared to the Irwin parabola [45] for un-bridged materials. A schematic representation of the crack tip bridging process is also included.

Figure 7. Percentage of fractured binder in the crack path as a function of the distance from the crack tip as obtained by inspection of the FIB sequential images.

Figure 8. Bridging stress distribution as a function of the crack opening displacement as calculated from expressions (6) and (7).

Figure 9. Estimated R-curve behavior for the investigated cemented carbide. Black points correspond to the estimated K_R values according to equation (2), while the black line is obtained after a best-fitting of such points according to equation (8), proposed by Ramachandran and Shetty [54] for describing R-curve response of ceramic/metal materials.

LIST OF TABLES

Table 1. Microstructural parameters for the investigated material.